

FINITE-ELEMENT MODEL OF THE INDENTATION FOR YBCO-BASED SUPERCONDUCTOR THIN FILMS

MODEL KONČNIH ELEMENTOV ZA VTISKOVANJE TANKIH PLASTI SUPERPREVODNIKA YBCO

Osman Culha¹, Ilyas Turkmen¹, Mustafa Toparli², Erdal Celik²

¹Celal Bayar University, Department of Materials Engineering, Muradiye Campus, Manisa, Turkey

²Dokuz Eylul University, Department of Metallurgical and Materials Engineering, Tinaztepe Campus, Buca, Izmir, Turkey
osman.culha@cbu.edu.tr

Prejem rokopisa – received: 2012-10-16; sprejem za objavo – accepted for publication: 2013-03-25

Superconducting films with poor mechanical properties are useless even if they possess good transport and flux-pinning properties. Since additive particles as pinning centers are important changes in a microstructure, their effect on the micromechanical properties such as Young's modulus and hardness have to be investigated with respect to the additional-particle type and quantity, using experimental and numerical methods. In this study, films were dip-coated onto (001) SrTiO₃ (STO) single-crystal substrates with metalorganic deposition using the trifluoroacetate (TFA-MOD) technique. The phase analysis and the microstructure of the superconducting thin films were determined with an X-ray diffractometer (XRD) and a scanning electron microscope (SEM). The mechanical-property variations of the pure YBCO and the YBCO thin films with Mn (reacting as BaMnO₃) were experimentally obtained with nanoindentation techniques. Thus, the BaMnO₃ nanoparticle effects on the structural and mechanical properties of the films were observed. According to the nanoindentation results, the Young's modulus and indentation hardness of the films decreased from 88.54 GPa to 76.47 GPa and from 12.51 GPa to 3.88 GPa, respectively, depending on the additive particles. In addition, the finite-element modeling (FEM) of the indentation was applied to estimate the failure stress/stress distribution relation at the contact region between the indenter and the surface of a YBCO-based thin film, obtaining the same force/penetration depth curve as with the indentation experiment. According to these main aims of FEM, the mesh-design effect, material properties and the boundary condition of the axisymmetric model were chosen and optimized to obtain the mechanical results of the instrumented indentation.

Keywords: superconducting films, mechanical properties, nanoindentation, finite-element modelling, stress distribution

Superprevodne tanke plasti s slabimi mehanskimi lastnostmi so neuporabne, čeprav imajo dobre transportne lastnosti in zmožnost zadrževanja toka. Ker so dodani delci kot mesta zadrževanja pomembna sprememba v mikrostrukturi, je treba z eksperimentalnimi in numeričnimi metodami raziskati njihov vpliv na mikromehanske lastnosti, kot sta Youngov modul in trdota, v odvisnosti od vrste in količine dodanih delcev. V tej študiji so bile mono- kristalne tanke plasti (001) SrTiO₃ (STO) s potapljanjem obložene s kovinsko-organskim nanosom z uporabo tehnike s trifluoroacetatom (TFA-MOD). Fazna analiza in mikrostruktura superprevodnih tankih plasti sta bili določeni z rentgenskim difraktometrom (XRD) oziroma z vrstičnim elektronskim mikroskopom (SEM). Spreminjanje mehanskih lastnosti čistega YBCO in tankih plasti YBCO z Mn (reagira kot BaMnO₃) je bilo eksperimentalno določeno z nanovtiskovanjem. Opaženi so bili učinki nanodelcev BaMnO₃ na strukturne in mehanske lastnosti plasti. Na podlagi rezultatov nanovtiskovanja sta se Youngov modul in trdota plasti zmanjšala iz 88,54 GPa na 76,47 GPa oziroma iz 12,51 GPa na 3,88 GPa, odvisno od dodanih delcev. Dodatno je bilo uporabljeno tudi modeliranje vtiskovanja s končnimi elementi (FEM) za določanje porušitvene razporeditve napetosti v področju stika vtisnega telesa in površine tanke plasti na osnovi YBCO, da bi dobili krivulje sila – globina vtiskovanja pri preizkusu vtiskovanja. Skladno s ciljem FEM-modela, je bil izbran učinek oblike mreže, lastnosti materiala in robni pogoji za osnosimetrični model in izvršeno je bilo optimiranje glede na dosežene rezultate pri mehanskem instrumentiranem vtiskovanju.

Gljučne besede: superprevodne tanke plasti, mehanske lastnosti, nanovtiskovanje, modeliranje s končnimi elementi, razporeditev napetosti

1 INTRODUCTION

Since the discovery of high- T_c superconductors, numerous researchers focused on their electric properties. The production effect and the critical-current density (J_c) dependence on the external magnetic field and on the temperature in high- T_c superconductor (HTS) YBCO films have been widely investigated.¹⁻⁷ The results demonstrate a high potential for an application of YBCO films in power devices such as fault current limiters (FCL) and motors. J_c depends on the vortex-pinning capability of a film, the optimization of which is currently achieved by controlling the microstructure and the defect distribution (BaMeO₃ as a nanorod and dot) in a film. However, increasing the pinning-center density

up to the value, at which the distance between the nearest centers reaches the coherence length will severely deteriorate the mechanical properties of the films. Thus, it may occur that for many of the HTS thin-film applications requiring a high critical-current density, the limiting factor will no longer be the critical-current density magnitude but the mechanical strength against the body forces caused by flux pinning. The mechanical strength makes a crucial contribution to the stability and credibility of any device based on this form of materials.⁸ In addition, the mechanical properties are also very important for the final industrial application.

In the literature, there have been several reports on their hardness, bending strength and internal friction. A precise knowledge of the elastic and deformation beha-

viour is a prerequisite for a successful production and operation of such devices. However, very little information on the elastic-to-plastic transition is available in the literature.^{9–11} On the other hand, nanoindentation has been used routinely in the mechanical characterization of thin films and thin-surface layers in recent years.¹² The technique applies a programmed function of an increasing and decreasing load to the surface of interest with an indenter of a well-defined shape, continuously measuring the indenter displacement (**Figure 1**). The advantage of this method is that the mechanical information, such as the elastic modulus, can be obtained through an analysis of the load-displacement behavior using only the coating of the material to be tested on a substrate made from a different material. This makes it an ideal tool. The technique has been used to assess the elastic and plastic properties of coatings on a range of substrates, but there are limitations in measuring the properties of much thinner coatings, particularly when elastic properties are required.^{13,14} For the coatings with a thickness of a few hundred nanometers, it has been suggested that extrapolating the properties determined for a range of peak loads or indenter displacements to zero load/depth can be used to determine the coating-only properties. With high-quality sharp indenters it is possible to assess coatings down to the thickness of 100 nm using this method.¹⁵

The indentation-system frame stiffness and the diamond tip shape were carefully calibrated with a fused-silica test sample, using the standard Oliver and Pharr method (1992), before and after the measurements with no change for either of them. Nano-indentation load (P) vs. displacement (h) curves were then recorded for each indent and only the ones showing evidence of a plastic deformation (i.e., the loading and unloading curves are different) were used in the analysis of Young's modulus using the above methods.^{15–18} In addition, most of the previous studies about the depth-sensing nano-indentation technique demonstrate that: to extract the mechanical properties of the coatings or films from the indentation test, we should limit the indentation depth to less than 10–20 % of the film thickness.^{19,20} As we know, during the nanoindentation experiments, especially when the indentation depth is about 100–1000 nm, size-scale-dependent indentation effects become important. These possible size-scale-dependent effects on the hardness have been modeled using higher-order theories^{21–23} and these effects can also be related to the bluntness of the nominally sharp indenters.^{24,25} For the cases when the tip bluntness is on the same order as the indentation depth, Borodich and Keer²⁴ proposed fundamental relations for depth of indentation, size of contact region, load, hardness, and contact area for various boundary conditions. If the indentation is sufficiently deep (typically deeper than 1 μm), then the scale-dependent effects become small and negligible. Therefore, the limitation of the indentation depth to less than 10–20 % of the film thickness

for the films with the thickness measured in micrometers is not a good rule. However, when the indentation depth is deeper than 1 μm , the deformation of the substrate has an effect on extracting the mechanical properties of the film from the indentation test for very thin films. Saha and Nix²⁶ examined the effects of the substrate on determining the hardness and elastic modulus of thin films with nanoindentation. They found that the effect of the substrate hardness on the film hardness was negligible in the case of soft films and the substrate hardness affected the measured film hardness in the case of a hard film on a soft substrate.

Compared to hardness, the nanoindentation measurement of the elastic modulus of thin films was more strongly affected by the substrate. Recently, with respect to an elastic-plastic film applied to an elastic substrate system, some researchers^{23,27,28} have proposed the techniques that allow us to extract a film's elastic-plastic properties, taking into account the influence of the elastic substrate from a conical indentation test using the finite-element method (FEM). In this study, elastic properties and the limits (E and σ_f) of YBCO-based films with/without BaMnO_3 defects as pinning centers were designated with the finite-element method (FEM) and nanohardness experiments according to the theory of indentation. Furthermore, failure (σ_f), contact-deformation characteristics, stress distribution near the contacts of the films depending on the amount of formed BaMnO_3 particles were obtained using an algorithm with FEM and a comparison between the experimental and simulation results of the nanoindentation.

2 EXPERIMENTAL PROCEDURE

Initially, (100) STO single-crystalline substrates with dimension of 10 mm \times 10 mm \times 0.75 mm were rinsed in acetone using a standard ultrasonic cleaner. After that, the solutions were deposited on the substrates using a dip-coating process with a withdrawal speed of 0.3 cm/s in a vacuum atmosphere. The deposited gel films were converted to an epitaxial pure YBCO and a YBCO film with BaMnO_3 nanoparticles through a combination of calcining and heat-treatment procedures. After that, the structural development of the produced thin films was investigated with the X-ray diffraction (XRD-Rigaku D/MAX-2200/PC) patterns that were recorded using the $\text{Co K}\alpha$ irradiation (the wavelength, $\lambda = 0.178897$ nm), with the scanning range between $2\theta = 10^\circ$ and 90° . The surface topographies and additional-particle effects on the microstructure of the films were examined with a high-resolution scanning electron microscope SEM (JEOL JSM 6060). The hardness and Young's modulus of the produced thin films were measured under the peak load of 300 μN three times with the CSM Berkovich nanoindentation tester (the loading-unloading test mode) to determine the additional-particle effects on the mechanical properties.

3 INDENTATION MODELING OF YBCO-BASED THIN FILMS

A simulation of YBCO-based thin-film indentation analysis exposed very important mechanical properties such as the maximum (fracture-fracture) strength that influenced the mechanical stability of the coated superconductor under service conditions. The elastic modulus and hardness of YBCO-based thin films could be determined from the instrumented indentation with the loading-unloading curves. However, the maximum stress, the stress-strain relationship, the substrate and the thickness effect on the characteristic loading-unloading curves could not be obtained from the experimental results. At this time, researchers used a simulation and finite-element modeling with the developed algorithms. Normally, until the 2000 s, a finite-element analysis of an indentation problem was applied to bulk ceramic and metallic-based materials. However, after the development of thin-film technologies and materials had increased, the determination of mechanical properties of films and coatings became more focused. For instance, thin-film-based technologies provide for a higher performance, a

higher density and a smaller overall size of a micro-system package. Although thin films are increasingly used for the sake of performance, functionality and size, it is important to understand the mechanical behavior of thin films to address the reliability concerns.

The indentation analysis of YBCO-based thin films was started with a design of an axisymmetric model. A diamond conical surface with a half-apex angle of 70.3° was used to model the widely used Berkovich indenter. In addition, the thicknesses of YBCO-based thin films and substrates were 300 nm and 5000 nm, respectively, and the ratio of the film thickness to the substrate was

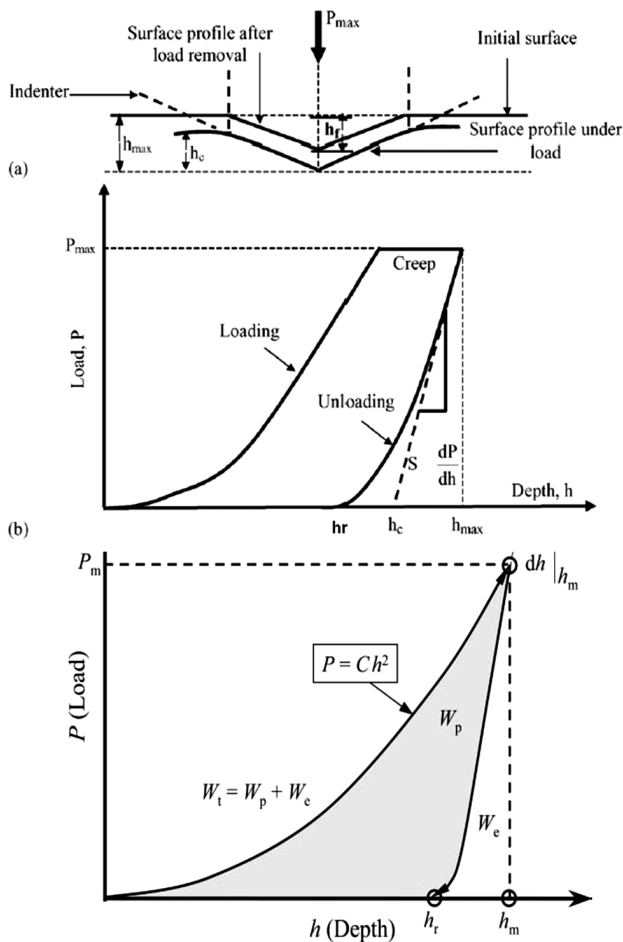


Figure 1: Characteristic indentation curve and representation of the parameters

Slika 1: Značilna krivulja vtiskovanja in predstavljeni parametri

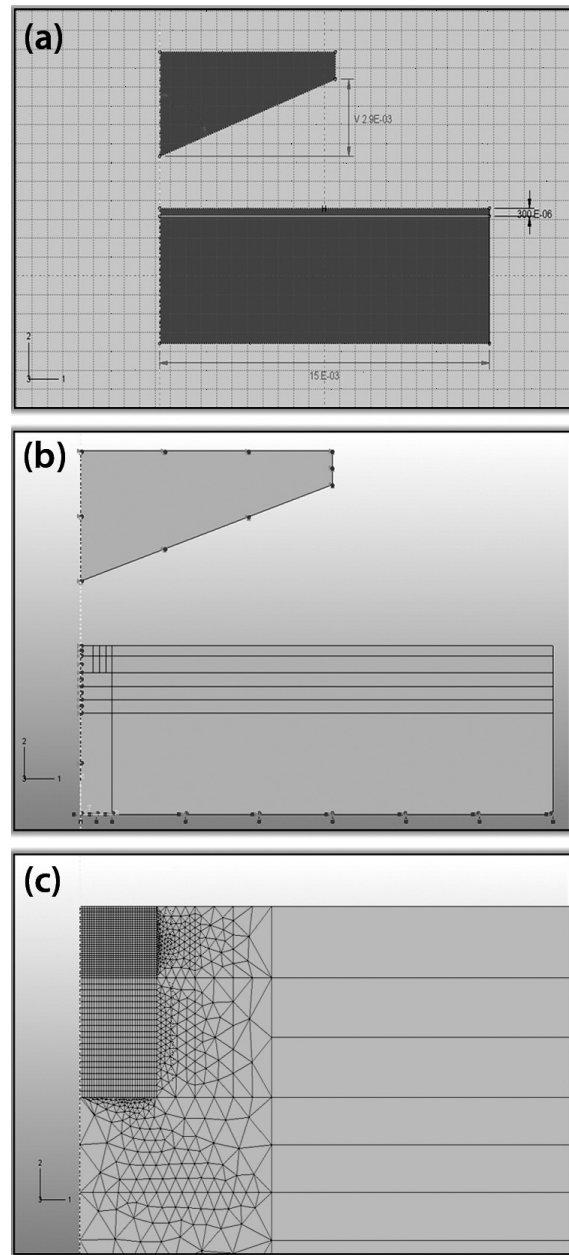


Figure 2: Finite-element model of YBCO-based thin films on an STO single-crystal substrate

Slika 2: Model končnih elementov tanke plasti na osnovi YBCO na monokristalni podlagi STO

6 % in this model. The substrate dimensions (both width and height) are taken to be at least 16 times larger than those of the film, so as to simulate a semi-infinite substrate (**Figure 2a**). On the other hand, four different material inputs were loaded to the model as a pure YBCO thin film, a YBCO thin film with 0.05 g Mn, a YBCO thin film with 0.10 g Mn and a YBCO thin film with 0.15 g Mn (BaMnO_3). The input data of the material properties of the axisymmetric thin-film model with a substrate and an equivalent cone are listed in **Tables 1** and **2**. Elastic modules were experimentally determined from the indentation unloading curves for four different YBCO-based thin-film models. So, the determined elastic modules were loaded with Poisson's ratio as the material elastic properties in the finite-element simulation. While fixing the elastic properties presented in **Table 2** for each sample, the maximum stresses (failures) of YBCO-based thin films were changed to determine the same penetration force/depth curve with the experimental indentation analysis.

The properties of the contact region between the indenter and the surface of a thin film/ substrate system could be designed in the assembly and interaction modulus of the Abaqus package program. The contact areas of YBCO-based thin films were divided into partitions. As known from the indentation-analysis theory, a fine-mesh design could be applied to the mesh part so as to create the partitions near the contact region. The contact regions of YBCO-based thin films were calculated as the dimensions of 300 nm \times 400 nm (thickness \times length). After this area determination (depending on the indentation depth), the whole model began to partition from the contact region to the substrate with dimensions of 500 nm and 400 nm, respectively (**Figure 2b**). This partitioned model can be used for different element-type

and region determinations for a fine-mesh design of a contact area. At the same time, interaction properties for the indenter and the film surface are established as the finite-sliding formulation and surface-to-surface constraint-enforcement method. The contact property of the entire model was assumed to be tangential, being frictionless between the indenter and the surface of a film.

As the main aim of the study was to obtain the stress distributions and force-depth curves of YBCO thin films, the mesh design of the entire model became important, especially when a problematic region included a contact between two separated surfaces. As we already know, the instrumented indentation analysis was carried out with a diamond indenter that penetrated the surface of a thin film at the nanoscale, deforming the contact region, not the whole surface, plastically under the applied load. The importance of a divided surface near a contact region required very correct and sensitive results for simulated loading-unloading curves of YBCO-based thin films. For that reason, the elements were the finest in the central contact area and became coarser outwards for the entire model and a magnified view of the contact region can be seen in **Figure 2**. According to **Figure 2c**, the contact region was meshed as a structured CAX4R element type, A-4 node bilinear axisymmetric quadrilateral, reduced integration and hourglass control with 2, 4, 8, 16, 32 and 40 numbers for a determination of the indentation depth and load dependency on the mesh-element number. In this model, as presented in **Figure 2c**, the contact-region size of YBCO-based thin films was 300 nm \times 400 nm. When the element number increased from 2 to 40, the element size was decreased from approximately 200 nm to 10 nm. The smallest element size and the total element number were 10 nm and 3764, respectively, which enabled an accurate determination of the real-impression size.

Table 1: Indentation-experiment results for YBCO-based superconducting thin films

Tabela 1: Rezultati eksperimentalnega vtiskovanja v superprevodno plast na osnovi YBCO

Material	Force (μN)	Max. depth (nm)	Res. depth (nm)	Film thickness (nm)	Hardness (HV)	Indentation hardness (GPa)	Young's modulus (GPa)
Pure YBCO thin film	300	40.24 ± 6.4	30.12 ± 7.8	292 ± 9	695 ± 28	12.51 ± 4.8	88.54 ± 3.1
YBCO thin film with 0.05 g Mn		42.32 ± 9.4	32.11 ± 8.7	297 ± 5	525 ± 16	8.21 ± 1.2	83.41 ± 1.8
YBCO thin film with 0.10 g Mn		42.45 ± 5.9	33.53 ± 4.4	294 ± 6	495 ± 21	5.75 ± 1.1	79.11 ± 1.9
YBCO thin film with 0.15 g Mn		47.04 ± 6.1	37.48 ± 5.7	305 ± 8	454 ± 18	3.88 ± 0.8	76.47 ± 1.3

Table 2: Material properties of the entire model

Tabela 2: Lastnosti materiala za celoten model

Material type	Elastic modulus (GPa)	Poisson ratio (ν)	Maximum stress (GPa)	Ratio of maximum stress to elastic modulus
Pure YBCO thin film	88.54	0.261	7.50–9.50	0.0847–0.1073
YBCO thin film with 0.05 g Mn	83.41		6.50–9.00	0.0779–0.1079
YBCO thin film with 0.10 g Mn	79.11		5.00–6.75	0.0632–0.0853
YBCO thin film with 0.15 g Mn	76.47		2.75–4.25	0.0360–0.0556
STO substrate	278	0.238	–	–
Equivalent cone	1040	0.07	–	–

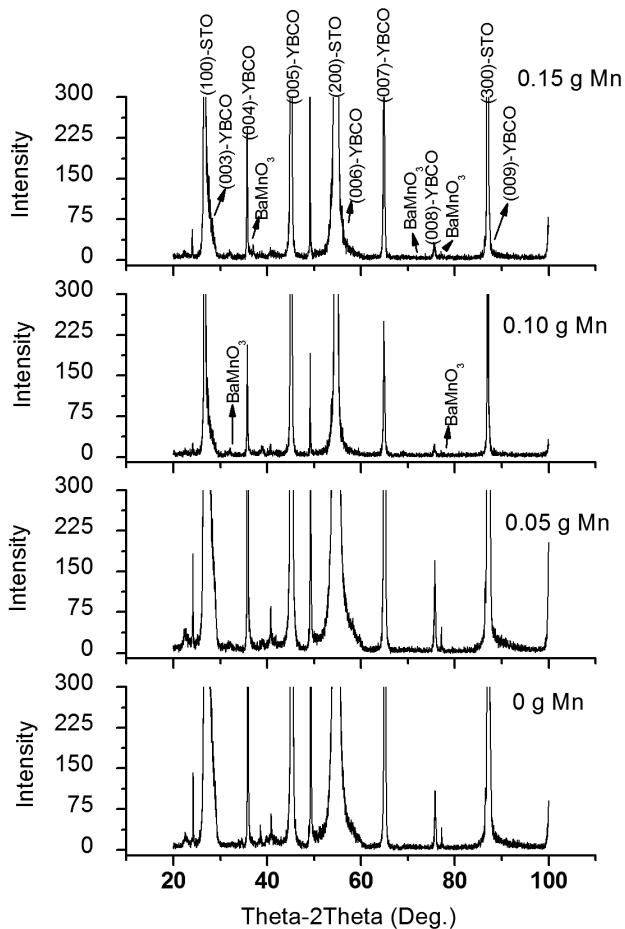


Figure 3: Phase analysis of YBCO-based superconductor thin films with additional particles

Slika 3: Fazna analiza superprevodne tanke plasti na osnovi YBCO z dodanimi delci

4 RESULTS AND DISCUSSION

4.1 Characterization of YBCO-based thin films

Details of the phase analysis of YBCO-based thin films are shown in **Figure 3** relating to the pure YBCO, and the YBCO with 0.05 g, 0.10 g and 0.15 g of BaMnO_3 nanoparticles on the STO single-crystal substrate. XRD patterns illustrate that YBCO films have (001) and parallel plane reflections for the pure YBCO thin film. The major diffraction peaks corresponding to the (001) parallel plane was developed. In addition, no second phases such as $\text{Y}_2\text{Cu}_2\text{O}_5$, BaF_2 and CuO were found, and only the pure YBCO phase was formed. Apart from that, BaMnO_3 perovskite peaks with a low intensity were determined on account of the Mn doping effect. On the other hand, the surface analysis of YBCO-based thin films indicated that structural defects could react as nanodots or nanoparticles (due to the Mn addition) along the c -axis of a YBCO film as presented in **Figure 4**. Since Mn reacts with Ba and a BaMnO_3 perovskite structure forms in the YBCO film during the heat-treatment process, the microstructures of superconducting thin films were changed as expected.

4.2 Instrumented indentation results of YBCO-based thin films

Since the general purpose is to determine the mechanical properties such as the Young's modulus and hardness of the pure YBCO thin film and the YBCO thin films with a Mn addition (Mn reacts as BaMnO_3), an instrumented nanoindentation test was used. At this time, the importance of the applied load became apparent. The indentation response of YBCO-based thin films on the

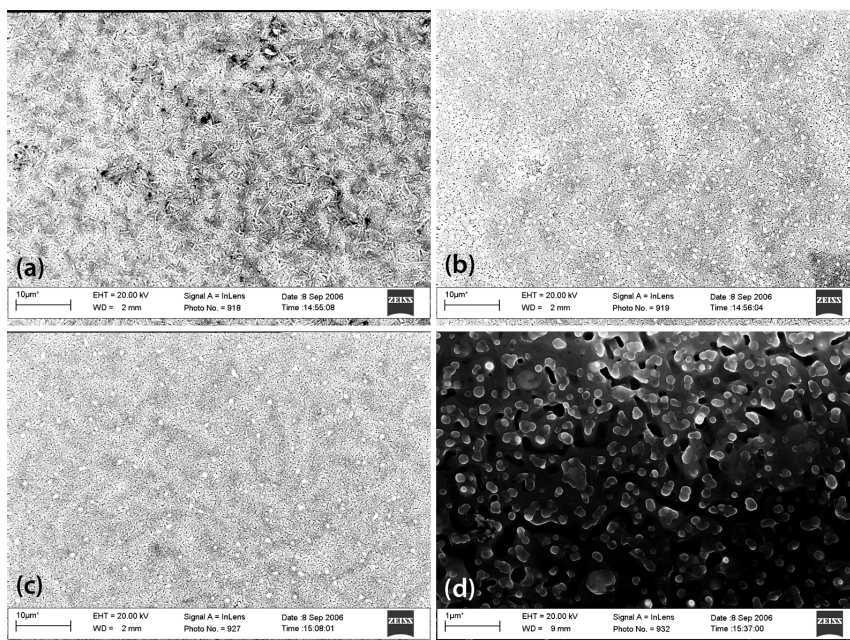


Figure 4: Surface analysis of YBCO-based superconductor thin films with additional particles

Slika 4: Analiza površine superprevodne tanke plasti na osnovi YBCO z dodanimi delci

STO substrate is a complex function of the elastic and plastic properties of both the film and the substrate and it is crucial to understand how the intrinsic mechanical properties of the film can be determined from the overall mechanical response of the film/substrate system. As the values of the elastic modulus and hardness, determined from indentations, do not depend on the value of h (indentation depth) and, therefore, on the value of the maximum load, the indentation depth should not exceed 10–20 % of the film thickness, otherwise the results will be affected by the properties of the substrate. Another parameter that can influence the indentation test is the surface roughness. It has a very active role in the indentation experiment at the nanoscale. If the surface roughness is bigger than the maximum indentation depth for the applied load, the curve has a very scattered loading and unloading part. According to the surface analysis, the surface roughness of the pure YBCO thin film is (21 ± 5) nm.

As presented in **Table 1**, the ratio of the indentation depth to the film thicknesses is applicable for the instrumented indentation with the 300 μ N applied load. The smoothing procedure was applied to all of the instrumented indentation results of the samples. The loading-unloading (load-displacement) curves of YBCO thin films under the 300 μ N applied peak load are shown in **Figure 5**, at the nanometer scale, three times and the total test time was 60 s. The maximum and residual indentation depths of the YBCO thin film were increased from (40.24 ± 6.4) nm to (47.04 ± 6.1) nm and from (30.12 ± 7.8) nm to (37.48 ± 5.7) nm, respectively, by increasing the Mn content in the structure (**Table 1**). The ratios of the indentation depth to the film thickness of the YBCO thin film, the YBCO with 0.05 g Mn, the YBCO with

0.10 g Mn and the YBCO with 0.15 g Mn were 13.78 %, 14.14 %, 14.43 % and 15.04 %, respectively. Furthermore, the elastic modulus and instrumented hardness of YBCO thin films were decreased from (88.54 ± 3.1) GPa to (76.47 ± 1.3) GPa and from (12.51 ± 5.1) GPa to (3.88 ± 0.8) GPa under the 300 μ N applied load as listed in **Table 1**. The loading and unloading parts of the curves have some fluctuations due to the surface roughness and porosity of YBCO-based thin films. For that reason the standard deviations were added to all the indentation-test characteristics, such as the maximum indentation depth, the residual depth, the elastic modulus and the instrumented hardness of the films.

According to the results, the indentation hardness of the films decreased with the increasing Mn content in the film structure. Depending on the Mn content, the maximum indentation depth, the residual depth and the indentation hardness were changed scientifically. Since the Mn content increased in the microstructures of YBCO-based films, the intensity of BaMnO_3 phases in the X-ray analysis increased. Furthermore, the SEM analysis showed that the BaMnO_3 phase structure dispersed and agglomerated in the YBCO thin-film structure. So, the characteristic indentation curves of YBCO-based thin films changed depending on the Mn content and the BaMnO_3 phase structure. As expected, BaMnO_3 reacted as a defect, becoming the pinning center in the structure. When the defect concentration increased due to the increased Mn content, the stability of the structure and interatomic bonding mechanism changed to particle-doped YBCO-based thin films. Although the lattice parameter was very close to YBCO, the BaMnO_3 based structure in YBCO thin films caused some distortion (the residual stress) and irregularities. Although the indenta-

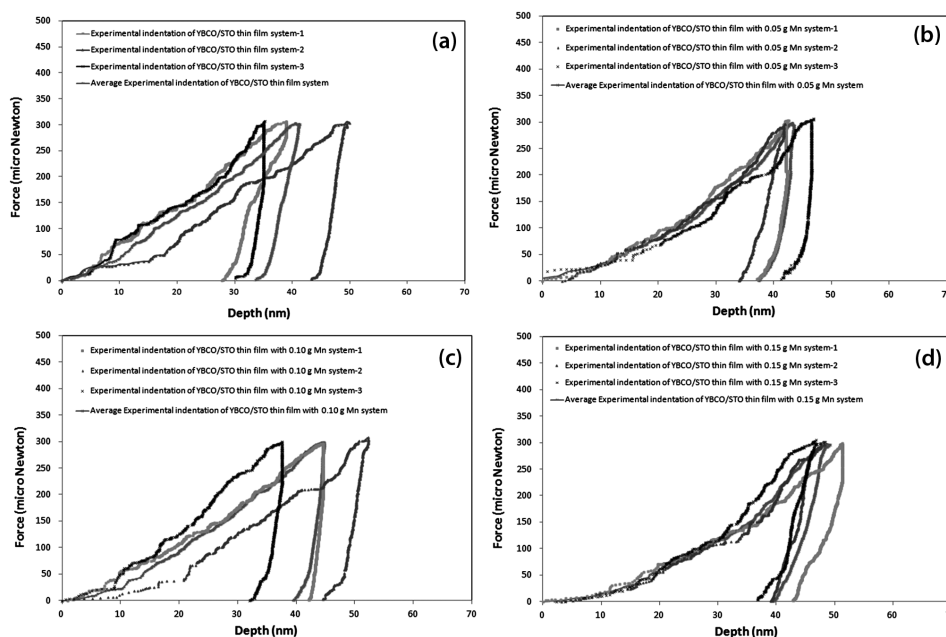


Figure 5: Indentation curves of YBCO-based thin films on the STO single-crystal substrate

Slika 5: Krivulje vtiskovanja tanke plasti na osnovi YBCO na monokristalni podlagi STO

tion load was fixed at 300 μN , the indentation hardness was decreased as if the indentation size effect had influenced the mechanical properties. Since the hardness is accepted as an inherent material property, it should not vary with the indentation load and size but can change with different phase formations. A decrease in the hardness due to the increasing BaMnO_3 content in the YBCO thin-film structure caused differences in the indentation depth. According to this explanation, it can be concluded that the pure YBCO thin film is harder and more brittle than the BaMnO_3 films. As presented in **Figure 6**, the indentation hardness of YBCO-based thin films decreased from 12.51 GPa to 3.88 GPa depending on the Mn content in the structure. The elastic-modulus variation of YBCO-based thin films is also demonstrated in **Figure 6**. Although hardness was very sensitive to the maximum indentation depth and thickness ratio of the samples, changing from 12.51 GPa to 3.88 GPa, the elastic modulus of YBCO-based thin films did not show any sharp decrease. However, as listed in **Table 1**, the elastic modulus of the pure YBCO, the YBCO with 0.05 g Mn, the YBCO with 0.10 g Mn and the YBCO with 0.15 g Mn was 88.54 GPa, 83.41 GPa, 79.11 GPa and 76.47 GPa, respectively. However, the references about the mechanical properties of this material, particularly the yield strength and the stress-strain curve, are scarce.

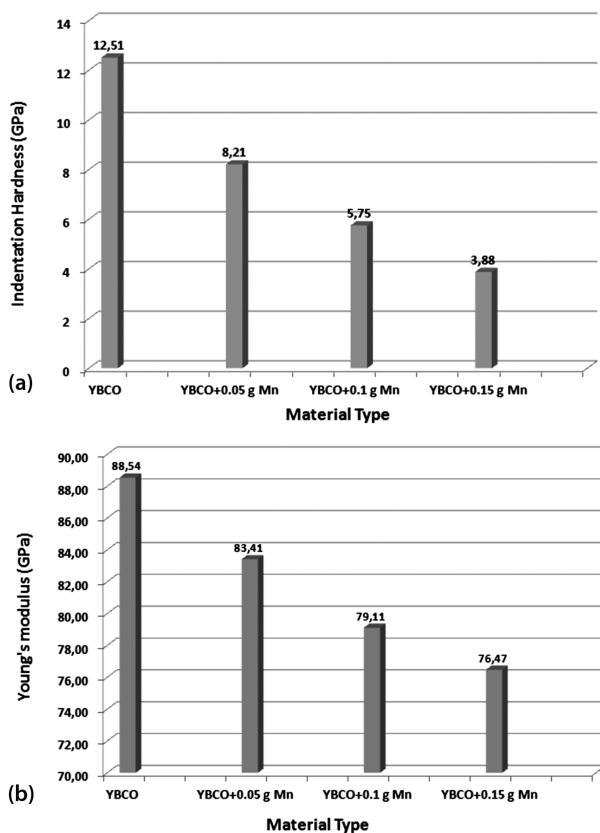


Figure 6: Indentation-hardness and elastic-modulus variations of YBCO-based thin films

Slika 6: Spreminjanje trdote in modula elastičnosti tanke plasti na osnovi YBCO

The mechanical properties (the hardness, the Young's modulus and the fracture toughness) of YBCO samples were examined with the techniques such as ultrasound²⁹ X-ray diffraction³⁰ and nanoindentation.³¹ The reported values of the Young's modulus for Y-123 are within the range of $E = 40\text{--}200$ GPa. This large scatter may be due to the residual porosity and poor contact between the grains.³² Other authors,³³ also using nanoindentation, reported a value of $E = 171\text{--}181$ GPa for the YBCO samples textured with the Bridgman technique, which is in agreement with Johansen, who applied between 30 mN and 100 mN. Nanohardness values in the range of 7.8–8.0 GPa at the maximum loads of 30 mN were recently reported by Lim and Chaudhri³⁴ for a bulk, single-crystal YBCO. Roa et al.³³ found a hardness value of (8.9 ± 0.1) GPa using nanoindentation on the YBCO samples textured with the Bridgman technique.^{32–37}

4.3 FEM results of indentation

The depth-sensing instrumented nanoindentation technique provided a continuous record of the variation in the indentation load and the penetration depth into the specimens. This technique has attracted considerable attention in recent years due to its high resolution at a low-load scale with respect to determining the elastic modulus and hardness of thin films. The importance of the mechanical stability of superconductor thin films with/without additional particles under service condition was exposed during the experimental work and finite-element modeling.

Additional particles behave as defect centers increasing the superconducting properties under a given temperature as explained above. While increasing superconducting properties with additional particles, in this study they are Mn (BaMnO_3) particles, the elastic modulus and the hardness of thin films decreased from 88.54 GPa to 76.47 GPa, 12.51 GPa and 3.88 GPa. However, the variations in the plastic properties of YBCO-based thin films with additional particles could not be determined with the instrumented indentation test. For that reason, the finite-element modeling of YBCO-based thin films with and without BaMnO_3 particles was carried out using the Abaqus 6.10-1 package program, taking into account the experimentally determined elastic properties of the films.

According to the depth analysis, indentation with a different element number and size for FEM, 40 elements with the element size of 10 nm, was chosen, due to its sensitivity at the nanometer scale, for the simulated loading and unloading curves of the pure YBCO thin film and the YBCO thin films with 0.05 g, 0.10 g and 0.15 g Mn. **Figure 7** shows that the simulated maximum and residual indentation depth variations for the four different YBCO-based thin films depend on the maximum stress rises under the 300 μN indentation load. According to the FEM indentation analysis, the maximum depth values decreased from 40.74 nm to 39.58 nm, 43.13 nm to 41.36 nm, 44.89 nm to 42.84 nm and

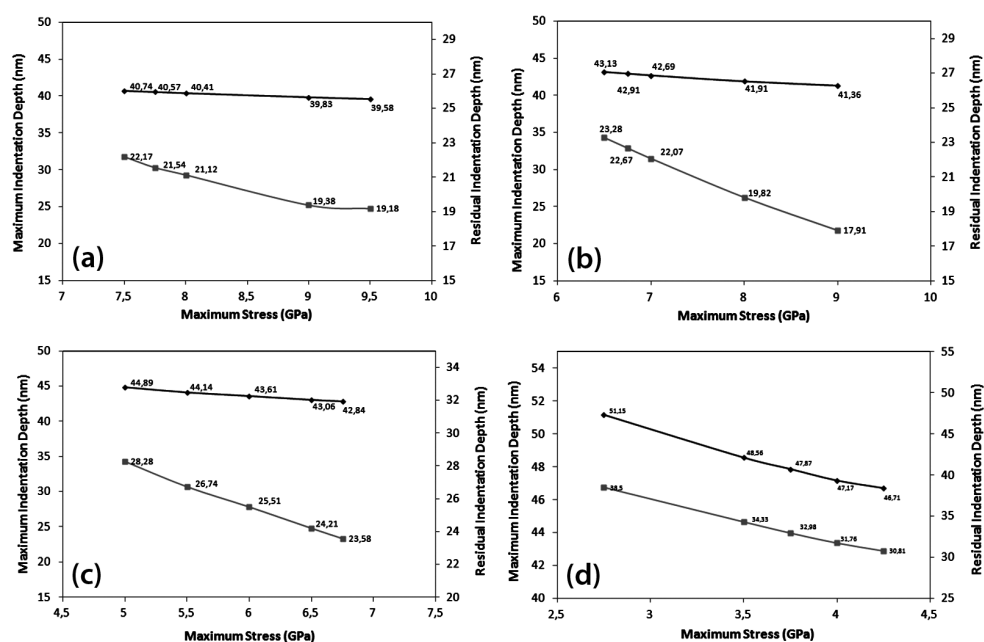


Figure 7: Depth analysis of the FEM model for YBCO-based thin film
Slika 7: Analiza globine s FEM-modelom pri tanki plasti na osnovi YBCO

51.15 nm to 46.71 nm due to an increase in the maximum stress value from 2.75 GPa to 9 GPa, respectively, for the material input data of the pure YBCO thin film and the films with Mn additions. On the other hand, the residual indentation depth of thin films decreased from 22.17 nm to 19.18 nm, 23.28 nm to 17.91 nm, 28.28 nm to 23.58 nm and 38.50 nm to 30.81 nm under the conditions of the same indentation-analysis input data (**Figures 7a, b, c and d**). However, the increases in the Mn content in the structures of YBCO-based thin films caused significant variations in mechanical properties. When the indentation results for the pure YBCO-based thin film and the film with the addition of 0.15 g Mn are compared under the same simulation conditions, it is found that the maximum and residual depths were increased from 40.74 nm to 51.15 nm and from 19.18 nm to 30.81 nm (**Figure 7**), respectively. It means that the ductility or the plastic-deformation properties of YBCO-based thin films increased due to the increased Mn content in the thin-film structure or the BaMnO₃ formation during the production procedure of the instrumented indentation.

Depending on the experimental set-up used to perform the indentation, the loading and unloading characteristics of the $P-h$ curve, and thus the material properties estimated from the analysis of the $P-h$ curves, could be obtained at varying levels of accuracy. Thus, the sensitivity of the estimated elasto-plastic properties to the variations in the input parameters obtained from the $P-h$ curves is an important issue. In the FEM study, the structural model of the instrumented indentation test was performed as an axisymmetric and, therefore, two-dimensional model. The indentation process is complex,

so simplifications and assumptions have to be made to achieve a low numerical cost but, of course, sufficient accuracy. For the time being, the problem is idealized: it was assumed that the surface of the specimen was ideally smooth, whereas in reality a certain roughness may be present as well, e.g., thin films of four different YBCOs. The indenter is an equivalent cone and, furthermore, isothermal conditions are adopted. The model set-up is described below. First, the appropriate boundary conditions were selected and the contact to be modeled was defined. All the simulations were carried out under the load-controlled conditions. Two reasons can be given for this: First, a real-indentation experiment is hard to execute under displacement-controlled conditions, i.e., up to the maximum displacement. Second, regarding the numerical cost and accuracy, neither displacement-controlled nor load-controlled experiments show an important advantage. A force-depth ($P-h$) curve is a straightforward characterization of indentation results that can be precisely obtained with the instrumented indentation equipment. As described above, the surfaces of YBCO-based thin films were ideally smooth. However, the instrumented indentation results are affected by the surface roughness of materials. Both loading and unloading parts of indentation curves can have more scattered data depending on the ratio of the indentation depth and roughness to the film thickness. **Figure 8a** presents both indentation and simulation results of pure YBCO-based thin films under the same condition of instrumented indentation. The same maximum penetration depth was obtained by setting E at 88.54 GPa and the maximum stress at 8.00 GPa for the experimental and simulation analyses (**Table 2**) for the pure YBCO thin film. The surface-roughness effect on the indentation

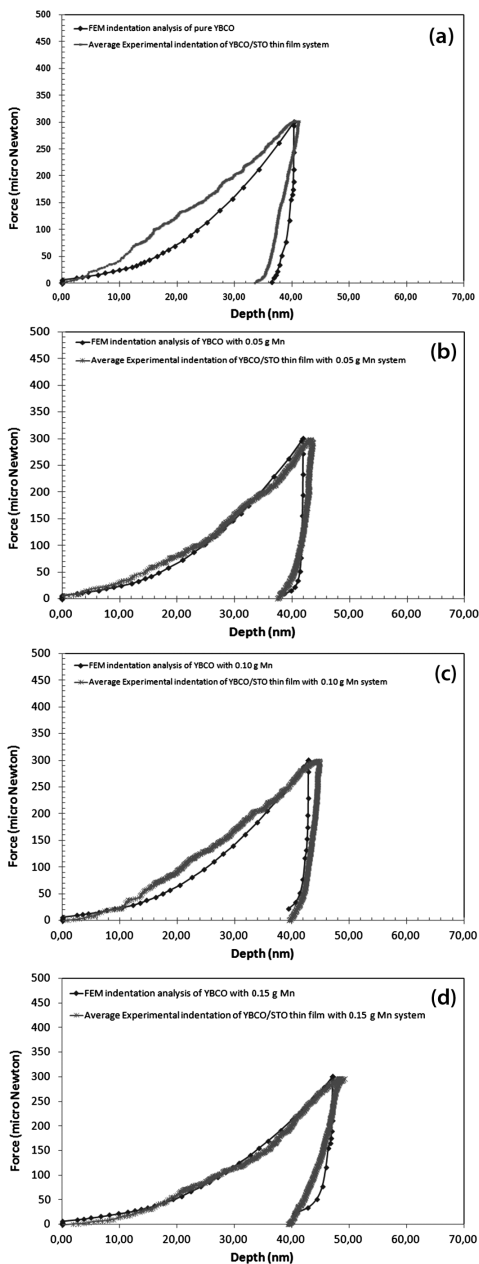


Figure 8: Comparison of experimental and simulation indentation curves

Slika 8: Primerjava eksperimentalnih in simuliranih krivulj vtiskovanja

simulation could not be seen due to the choice of an ideally smooth surface. According to the experimental indentation results, h_{\max} and h_r were (40.24 ± 6.4) nm and (30.12 ± 7.8) nm, respectively, for the $300 \mu\text{N}$ applied load. Similarly, the finite-element modeling of the pure YBCO-based thin-film indentation had the maximum and the residual indentation depths of 40.41 nm and 32.27 nm. Good agreement was found between the maximum indentation depth and the loading curves of pure YBCO-based thin films, having an error of 0.4 %. In addition, when the average experimental-indentation

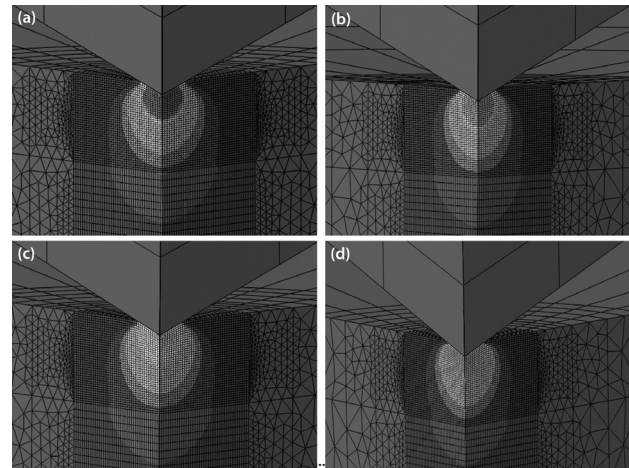


Figure 9: Stress-strain distributions on the contact regions between the indenter and the surfaces of the films

Slika 9: Razporeditev napetost – raztezek na področju kontakta med vtisnim telesom in površino tanke plasti

loading/unloading was considered, this error value was graphically obtained as 7 %, as presented in **Figure 8a**. This may be due to the differences in the maximum strength or due to the use of a constitutive model of both YBCO-based thin films, like the elastic/perfect plastic one without any strain-hardening exponent. On the other hand, **Figures 8b, c and d** show instrumented (the average for three different regions) and simulation indentation results for the YBCO-based thin films with 0.05, 0.10 and 0.15 g Mn under the $300 \mu\text{N}$ applied load. The experimentally determined maximum and residual indentation depths for YBCO-based thin films were (42.31 ± 9.4) nm and (32.11 ± 8.7) nm, (42.45 ± 5.9) nm and (33.53 ± 4.4) nm, and (47.04 ± 6.1) nm and (37.48 ± 5.7) nm, respectively. According to the FEM indentation results, the maximum and residual indentation depths for the YBCO-based thin film with Mn were 42.69 nm and 38.61 nm, 42.84 nm and 39.42 nm, and 47.17 nm and 40.43 nm, in line with the material input data from **Table 2**. When the average curves of the indentation were considered, the loading parts of the curves were much closer to the numerically determined ones.

With respect to the pure YBCO thin-film indentation results, the unloading part of the curves was separated as it was modeled without a strain hardening exponent. The strain hardening exponent of ceramics and, especially, oxide thin films was close to zero. As expected, ceramics- and oxide-based materials did not plastically deform and harden with deformation like the metals. Additionally, they showed brittle failures at the maximum stress. The main aim of the FEM study of indentation was to obtain the same experimental and numeric loading/unloading curves for YBCO-based thin films, while the elastic and plastic properties of the model were iterated according to **Table 2**. Depending on the material-property variation listed in **Table 2** for the FEM model, the maximum stress of YBCO-based films was

changed from 2.75 GPa to 9.50 GPa for different Mn additions. When the Mn content in the structure increased from 0 g to 0.15 g, allowing a BaMnO₃ formation, the maximum stress of the films decreased from 8.00 GPa to 4.00 GPa.

Stress distributions near the contact region of the indented material and the indenter give very important information about the simulation of the experimental indentation. The effects of the maximum depth, the residual depth and the film thickness on the substrate-film system under the applied load could be observed when the field-output request of the indentation analysis was undertaken depending on the steps of the simulations. **Figure 9** shows the Von Mises equivalent stress distributions for the pure YBCO-based thin film and the YBCO with 0.05 g, 0.10 g and 0.15 g Mn under the 300 μ N applied load at the contact regions. According to the analysis of the indentation, firstly, the indenter approached and made a contact with the surface. Secondly, the indenter was penetrating the surface until a load of 300 μ N was reached. As seen in **Figure 9**, the stress distribution shows yielded elements near the contact region for the indenter and the surface. It is understood that if an increase in the stress formation approaches the set maximum stress during the loading step, the plastically deformed part of the contact region can be analyzed easily when the unloading step of the simulation has finished. The maximum stresses for the pure YBCO and the ones with additional Mn were applied to the FEM model, described in **Table 2** as 7.50–9.50 GPa, 6.50–9.00 GPa, 5.00–6.75 GPa and 2.75–4.25 GPa, respectively. The same penetration force/depth curves were obtained with the instrumented indentation and simulation for the above films when the maximum stresses were loaded into the Abaqus 6.10-1 program in the following order: 8.00 GPa, 7.00 GPa, 6.75 GPa and 4.00 GPa.

5 CONCLUSION

In this study, finite-element modeling (FEM) of the indentation was applied to estimate the failure stress/stress distribution relation at the contact region between an indenter and a surface of YBCO-based thin films on an STO single-crystal substrate, and obtain the same force/penetration depth curve with an indentation experiment to determine the additional-particle effects on both structural and mechanical properties. So, the following results were obtained:

- XRD patterns show that YBCO films have (001) and parallel plane reflections for both the pure YBCO and the YBCO with a BaMnO₃ thin film.
- SEM micrographs indicate structural defects comprised of the nanodots or nanoparticles of BaMnO₃ along the *c*-axis of a YBCO film. These properties result in an enhanced pinning over the pure YBCO film.

- The calculated Young's modulus of YBCO-based thin films with/without BaMnO₃ decreased down to the range of 88.54–76.41 GPa, with the increased Mn content in the microstructure. In addition, the indentation-hardness values of the films were decreased from 12.51 GPa to 3.88 GPa depending on the Mn content.
- The finite-element-analysis results showed that the maximum, or failure, stress of YBCO-based thin films decreased due to the increased Mn content in the microstructure. The yield stresses of the pure YBCO thin film, the YBCO thin film with 0.05 g Mn, the YBCO thin film with 0.10 g Mn and the YBCO thin film with 0.15 g Mn were found to be 8.00 GPa, 7.00 GPa, 6.75 GPa and 4.00 GPa, respectively, by comparing the experimental work and numerical load-penetration-depth analysis under the applied load of 300 μ N.

6 REFERENCES

- ¹ G. Blatter, M. V. Feigelman, V. B. Geshkenbein, A. I. Larkin, V. M. Vinokur, Vortices in high-temperature superconductors, *Rev. Modern Phys.*, 66 (1994), 1125
- ² C. S. Pande, Microstructural aspects of high and low T_c Superconductor, *Mater. Phys. Mech.*, 2 (2000), 1
- ³ E. Sheriff, R. Prozorov, Y. Yeshurun, A. Shaulov, G. Koren, C. Chabaud-Villard, Magnetization and flux creep in thin YBa₂Cu₃O_{7-x} films of various thickness, *J. Appl. Phys.*, 82 (1997), 4417
- ⁴ T. Araki, I. Hirabayashi, Review of a chemical approach to YBa₂Cu₃O_{7-x} coated superconductors-metalorganic deposition using trifluoroacetates, *Superconducting Science and Technology*, 16 (2003), 71–94
- ⁵ T. Araki, T. Kato, T. Muroga, T. Niwa, T. Yuasa, H. Kurosaki et al., Carbon Expelling scheme and required conditions for obtaining high-Jc YBa₂Cu₃O_{7-x} film by metalorganic deposition using trifluoroacetates, *IEEE Transactions on Applied Superconductivity*, 13 (2003) 2, 2803–2808
- ⁶ E. Celik, E. Avci, Y. S. Hascicek, Growth Characteristic of ZrO₂ Insulation Coatings on Ag/AgMg Sheathed Bi-2212 Superconducting Tapes, *Mat. Sci. Eng. B*, 110 (2004), 213–220
- ⁷ X. M. Cui, B. W. Tao, J. Xiong, X. Z. Liu, J. Zhu, Y. R. Li, Effect of annealing time on the structure and properties of YBCO films by the TFA-MOD method, *Physica C*, 432 (2005), 147–152
- ⁸ A. Verdyan, Y. M. Soifer, J. Azoulay, E. Rabkin, M. Kazakevich, Nanohardness and Crack Resistance of HTS YBCO Thin Films, *Transaction and applied superconductivity*, 15 (2005) 2, 3585–3588
- ⁹ J. J. Roa, E. Jiménez-Piqué, X. G. Capdevila, M. Segarra, Nanoindentation with spherical tips of single crystals of YBCO textured by the Bridgman technique: Determination of indentation stress-strain curves, *Journal of the European Ceramic Society*, 30 (2010), 1477–1482
- ¹⁰ N. Güçlü, U. Kölemen, O. Uzun, S. Çelebi, Work of indentation approach for investigation of mechanical properties of YBCO bulk superconductor at cryogenic temperatures, *Physica C*, 433 (2005), 115–122
- ¹¹ O. Uzun, U. Kölemen, S. Çelebi, N. Güçlü, Modulus and hardness evaluation of polycrystalline superconductors by dynamic microindentation technique, *Journal of the European Ceramic Society*, 25 (2005), 969–977
- ¹² S. J. Bull, Nanoindentation of coatings, *Journal of Physics D: Applied Physics*, 38 (2005), 393–413

- ¹³ A. M. Korsunsky et al., On the hardness of coated systems, *Surface & Coatings Technology*, 99 (1998), 171–183
- ¹⁴ J. Chen, S. J. Bull, A critical examination of the relationship between plastic deformation zone size and Young's modulus to hardness ratio in indentation testing, *Journal of Materials Research*, 21 (2006), 2617–2627
- ¹⁵ J. Chen, S. J. Bull, On the factors affecting the critical indenter penetration for measurement of coating hardness, *Vacuum*, 83 (2009), 911–920
- ¹⁶ W. C. Oliver, G. M. Pharr, An Improved Technique for Determining Hardness and Elastic Modulus Using Load and Displacement Sensing Indentation Experiments, *J. Mater. Res.*, 7 (1992) 6, 1564–1583
- ¹⁷ A. E. Giannakopoulos, S. Suresh, Determination of elastoplastic properties by instrumented sharp indentation, *Scripta Materialia*, 40 (1999) 10, 1191–1198
- ¹⁸ F. Sen, E. Celik, M. Toparli, Transient thermal stress analysis of CeO₂ thin films on Ni substrates using finite element methods for YBCO coated conductor, *Materials and Design*, 28 (2007), 708–712
- ¹⁹ C. Gamonpilas, E. P. Busso, On the effect of substrate properties on the indentation behaviour of coated systems, *Materials Science and Engineering A*, 380 (2004) 1–2, 52–61
- ²⁰ N. Panich, Y. Sun, Effect of penetration depth on indentation response of soft coatings on hard substrates: a finite element analysis, *Surface and Coatings Technology*, 182 (2004) 2–3, 342–350
- ²¹ W. W. Gerberich, J. C. Nelson, E. T. Lilleodden, P. Anderson, J. T. Wyrobek, Indentation induced dislocation nucleation: the initial yield point, *Acta Materialia*, 44 (1996) 9, 3585–3598
- ²² N. A. Fleck, J. W. Hutchinson, A phenomenological theory for strain gradient effects in plasticity, *Journal of the Mechanics and Physics of Solids*, 41 (1993) 12, 1825–1857
- ²³ D. J. Ma, K. W. Xu, J. W. He, J. Lu, Evaluation of the mechanical properties of thin metal films, *Surface and Coatings Technology*, 116–119 (1999), 128–132
- ²⁴ F. M. Borodich, L. M. Keer, C. S. Korach, Analytical study of fundamental nanoindentation test relations for indenters of nonideal shapes, *Nanotechnology*, 14 (2003) 7, 803–808
- ²⁵ V. M. Kindrachuk, B. A. Galanov, V. V. Kartuzovl, S. N. Dub, On elastic nanoindentation of coated half-spaces by point indenters of non-ideal shapes, *Nanotechnology*, 17 (2006) 4, 1104–1111
- ²⁶ R. Saha, W. D. Nix, Effects of the substrate on the determination of thin film mechanical properties by nanoindentation, *Acta Materialia*, 50 (2002) 1, 23–38
- ²⁷ M. H. Zhao, N. Ogasawara, N. Chiba, X. Chen, A new approach to measure the elastic-plastic properties of bulk materials using spherical indentation, *Acta Materialia*, 54 (2006) 1, 23–32
- ²⁸ X. Chen, J. J. Vlassak, Numerical study on the measurement of thin film mechanical properties by means of nanoindentation, *J. Mater. Res.*, 16 (2001), 2974
- ²⁹ F. Sandiumenge, T. Puig, J. Rabier, J. Plain, X. Obradors, Optimization of flux pinning in bulk melt textured 1–2–3 superconductors; Bringing dislocations under control, *Adv. Mater.*, 12 (2000), 375
- ³⁰ S. Block, G. J. Piermarini, R. G. Munro, W. Wong-Ng, The bulk modulus and Young's modulus of the superconductor Ba₂Cu₃YO₇, *Adv. Ceram. Mater.*, 2 (1987), 601
- ³¹ T. H. Johansen, Flux-pinning-induced stress and magnetostriction in bulk superconductors, *Supercond. Sci. Technol.*, 13 (2000), 12
- ³² H. M. Ledbetter, M. W. Austin, S. A. Kim, M. Lei, Elastic constants and Debye temperature of polycrystalline yttrium barium copper oxide (YBa₂Cu₃O_{7-x}), *J. Mater. Res.*, 2 (1987), 786
- ³³ J. J. Roa, X. G. Capdevila, M. Martinez, F. Espiell, M. Segarra, Nanohardness and Young's modulus of YBCO samples textured by the Bridgman technique, *Nanotechnology*, 18 (2007), 385
- ³⁴ Y. Y. Lim, M. M. Chaudhri, Nanohardness mapping of the curved surface of spherical macroindentations in fully annealed polycrystalline oxygen-free copper, *Phys. Status. Solid. A: Appl. Res.*, 194 (2002), 19–29
- ³⁵ W. A. Ortiz, R. Zadorosny, W. A. C. Passos, P. C. de Camargo, C. M. Lepienski, Vortex matter in a thin film of YBCO with columnar indentations-very small and moderate field regimes, *Physica C: Superconductivity*, 437–438 (2006), 254–257
- ³⁶ F. Yu, K. W. White, R. Meng, Mechanical characterization of top-seeded melt-textured YBa₂Cu₃O_{7-δ} single crystal, *Physica C: Superconductivity*, 276 (1997) 3–4, 295–308
- ³⁷ Y. M. Soifer, A. Verdyan, I. Lapsker, J. Azoulay, AFM investigations of the morphology features and local mechanical properties of HTS YBCO thin films, *Physica C: Superconductivity*, 408–410 (2004), 846–847